7-1-2019

A Computationally Efficient U-Net Architecture for Lung Segmentation in Chest Radiographs

Barath Narayanan
University of Dayton

Russell C. Hardie
University of Dayton, rhardie1@udayton.edu

A Computationally Efficient U-Net Architecture for Lung Segmentation in Chest Radiographs

Barath Narayanan Narayanan* and Russell C. Hardie+
Department of Electrical and Computer Engineering
University of Dayton, Dayton, OH 45469, USA
Email: {narayananb1*, rhardie1+}@udayton.edu

Abstract **- Lung segmentation plays a crucial role in computer-aided diagnosis using Chest Radiographs (CRs). We implement a U-Net architecture for lung segmentation in CRs across multiple publicly available datasets. We utilize a private dataset with 160 CRs provided by the Riverain Medical Group for training purposes. A publicly available dataset provided by the Japanese Radiological Scientific Technology (JRST) is used for testing. The active shape model-based results would serve as the ground truth for both these datasets. In addition, we also study the performance of our algorithm on a publicly available Shenzhen dataset which contains 566 CRs with manually segmented lungs (ground truth). Our overall performance in terms of pixel-based classification is about 98.3% and 95.6% for a set of 100 CRs in Shenzhen dataset and 140 CRs in JRST dataset. We also achieve an intersection over union value of 0.95 at a computation time of 8 seconds for the entire suite of Shenzhen testing cases.**

Index Terms **– Chest Radiographs, Lung Segmentation, Convolutional Neural Networks, U-Net**

I. INTRODUCTION

Automated lung segmentation plays a crucial role in computer aided diagnosis. Chest Radiography (CR) is one of the most commonly utilized imaging modalities by radiologists. CRs are utilized for various diagnoses that include but are not limited to pneumonia, lung cancer, tuberculosis, etc. Segmentation of the lungs plays an important role in these diagnoses. Automated segmentation of lungs provides insights to radiologists and other doctors in terms of shape, size and other relevant geometrical properties. Shape, size and location of lung varies for each patient and with age, gender, health condition, and scanner utilized. This makes it challenging for automated segmentation. Accurate lung segmentation is valuable for radiologists and assists them during screening for various diseases.

Automated lung segmentation has been a research area attracting great interest. Several methods have been proposed in the literature to solve this problem [1-16]. In [1, 2], certain rule based anatomical methods are developed to segment the lungs. In [3], a pixel-based classification model (lung and not lung) is developed for segmentation of lungs. In [4-8], Active Shape Model (ASM) is used for automatic segmentation of lungs in CRs and Computed Tomography (CT) scans. In [13], anatomical atlases-based algorithm is presented for lung segmentation. In [14] and [15], ASM tuned and hybrid voting based approaches are presented for segmentation of lungs in CR.

In this research, we adopt deep learning based semantic segmentation for lung segmentation. Deep learning based semantic segmentation is providing state-of-the-art results in various applications including medical imaging applications [9-11]. These tasks include classification, segmentation and detection. U-Net has been a popular segmentation technique in the field of biomedical imaging [12]. In this research, we propose a U-Net based architecture for automated lung segmentation for **two** publicly available datasets thereby setting a benchmark for future research efforts. We evaluate our algorithmic approach by performing hold-out validation under two different test scenarios. We study the performance by utilizing a subset of cases from a given database for training and testing purposes respectively. Later, we also test the robustness of our model by training and testing on independent datasets.

The proposed U-Net model is developed based on Convolutional Neural Network (CNN) with no data augmentation. This type of automated lung segmentation would enhance the workflow of a radiologist. The proposed segmentation algorithm is computationally efficient and is relatively accurate compared to its benchmark algorithms. The proposed U-Net architecture computes lung masks for the entire suite of 100 test cases in about 8 seconds whereas approaches such as anatomical atlases [13] take about 20-25 seconds per case which indicates a speedup of 250x.

The remainder of this paper is organized as follows. Section 2 provides a brief description about the databases that are employed in this research. Section 3 presents the U-Net architecture proposed in this research. Section 4 presents the experimental results obtained using the proposed methods. Finally, conclusions are offered in Section 5.

II. Materials

Aforementioned, we study the performance of our algorithm under two different conditions. At first, we describe the scenarios in which we utilize independent databases to study the robustness of the proposed algorithm.

We train our algorithm using a private dataset provided by the Riverain Medical Group [4] with 160 CRs. However, the actual ground truth lung masks segmentation has not been provided for this dataset. We test our algorithm by evaluating the performance on a publicly available dataset provided by the Japanese Radiological Scientific Technology (JRST) [17]. The test dataset comprises 140 CRs mentioned in [4, 5]. Similar to our training dataset, ground truth lung segmentation for JRST dataset is not publicly available. We overcome this problem by utilizing the ASM results presented in [4] to serve as the ground truth for both training and testing purposes. ASM has provided state-of-the-art lung segmentation results for Riverain dataset and JRST dataset. Hence, we utilize the same as ground truth masks. Figure 1 shows a typical ASM result obtained using a CR from the JRST dataset. Table 1 presents the training and testing distribution in this scenario.

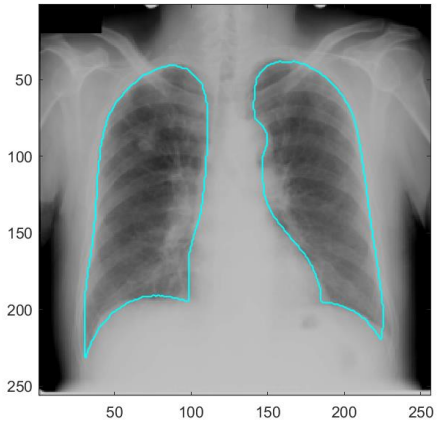

Figure 1: ASM results for the case 'JPCLN014' from JRST Dataset

Later, we investigate the performance of our proposed algorithm on the publicly available Shenzhen dataset [18, 19] where ground truth for lung segmentation is publicly available. Shenzhen dataset comprises 566 CRs with manual lung segmentation by domain experts. We randomly split the dataset into a group of **466** CRs and **100** CRs for training and testing purposes respectively. Figure 2 presents an example case from the Shenzhen dataset with ground truth lung mask. Table 1 presents the training and testing distribution in this scenario.

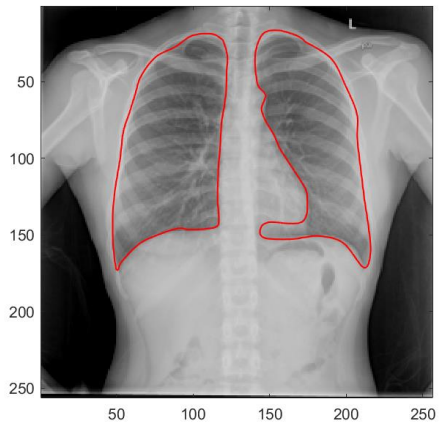

Figure 2: Manually segmented lung mask for a case from the Shenzhen Dataset

Table 1: Distribution of Training and Testing Datasets: Both Scenarios

Testing Scenario	Riverain **(ASM Truth)**		JRST **(ASM Truth)**		Shenzhen **(Manual Truth)**	
	Train	Test	Train	Test	Train	Test
Independent database	160	0	0	140	0	0
Same database	0	0	0	0	466	100

III. U-Net Architecture

Architecture of the segmentation tasks requires both encoding and decoding units. Encoding is implemented using a typical CNN which converts input images into a large number of feature maps with lower dimensionality [20]. Later, transposed convolution (deconvolution) operations are performed to produce segmentation masks with same dimensions as the input image. Thus, a large set of parameters are to be determined for segmentation-based tasks. For this research, we convert all the images to a size of 256×256. We utilize three stages of encoding and decoding in this research. Figure 3 presents the U-Net architecture implemented in this paper for lung segmentation. All the convolutional operations performed are 3×3 and max pooling layers are of size 2×2 with a stride of 2. Convolutional layer weights in the encoder and decoder are initialized using 'He' weight initialization method [21]. In addition, we must perform up-convolution and bridge convolution operations which will have additional parameters to train the network. Each deconvolution layer contains deconvolution and unpooling operations and it is implemented using bilinear interpolation [22]. Tables 2-5 list the parameters to be determined in each convolutional layer during encoding, decoding, bridge and up-convolution stages respectively. This type of U-Net architecture is implemented with the help of MATLAB's built-in function *unetLayers* [23]. We utilize 'Adam' optimization algorithm with an initial learning rate of 0.001 and we set the epochs to 200 with a mini

batch size of 16. Remove probability for dropout layer is set to be 0.5.

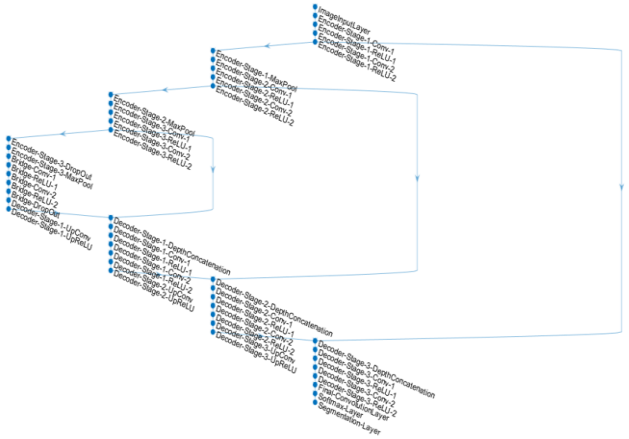

Figure 3: U-Net Architecture for Lung Segmentation in CRs

Table 2: Convolutional Layer Parameters during Encoding

Encoding Stages		Number of filters	Parameters (Excluding Bias)
Stage	Conv. #		
1	1	64	$3 \times 3 \times 1 \times 64$
1	2	64	$3 \times 3 \times 64 \times 64$
2	1	128	$3 \times 3 \times 64 \times 128$
2	2	128	$3 \times 3 \times 128 \times 128$
3	1	256	$3 \times 3 \times 128 \times 256$
3	2	256	$3 \times 3 \times 256 \times 256$

Table 3: Convolutional Layer Parameters during Decoding

Decoding Stages		Number of filters	Parameters (Excluding Bias)
Stage	Conv. #		
1	1	256	$3 \times 3 \times 512 \times 256$
1	2	256	$3 \times 3 \times 256 \times 256$
2	1	128	$3 \times 3 \times 256 \times 128$
2	2	128	$3 \times 3 \times 128 \times 128$
3	1	64	$3 \times 3 \times 128 \times 64$
3	2	64	$3 \times 3 \times 64 \times 64$

Table 4: Bridge Convolution Layer Parameters

Bridge Convolution #	Number of filters	Parameters (Excluding Bias)
1	256	$3 \times 3 \times 256 \times 512$
2	512	$3 \times 3 \times 512 \times 512$

Table 5: De-Convolutional Layer Parameters (used in Up-convolution)

Decoding Stage #	Number of filters	Parameters (Excluding Bias)
1	256	$2 \times 2 \times 256 \times 512$
2	128	$2 \times 2 \times 128 \times 512$
3	64	$2 \times 2 \times 64 \times 128$

IV. Experimental Results

In this section, we present the results obtained using the U-Net approach for the different databases utilized in this research. We also present the performance measure in terms of confusion matrix obtained using pixel-based classification approach. In addition, we present the segmentation results in terms of Intersection over Union (IOU) based on the obtained segmentation and ground truth.

First, we present the results obtained using independent database scenario. Training and testing distributions are as mentioned in Table 1. We evaluate the performance on a set of 140 CRs from the JRST database. Figure 4 presents the normalized confusion matrix obtained using pixel-based classification approach on test cases. Overall accuracy of **95.7%** is achieved in terms of classification of pixels as lung and not lung. An IOU value of **0.92** is obtained in terms of segmentation.

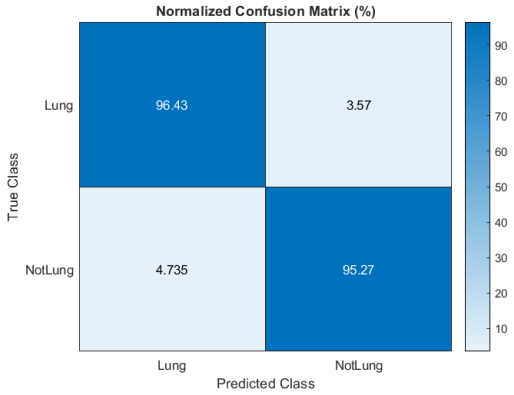

Figure 4: Normalized Confusion Matrix obtained for JRST Database

Figure 5 presents the result obtained for an example case using ASM and U-Net masks. Recollect, ASM based results serve as the ground truth for both Riverain and JRST database.

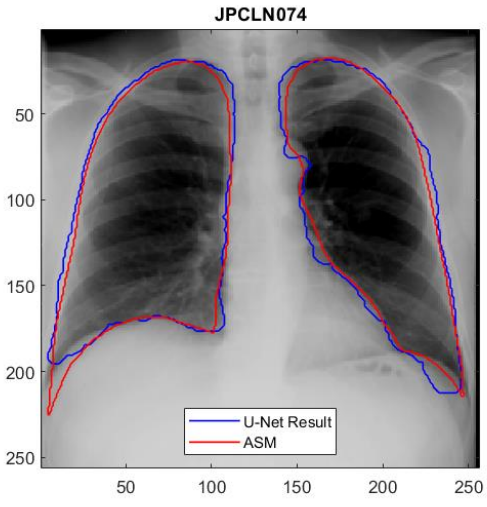

Figure 5: U-Net result obtained for an example case from the JRST Database

Now, we study the performance of the algorithm based on Shenzhen dataset. Aforementioned, we have the luxury of the manually segmented lung masks for Shenzhen dataset. We study the performance on a set of 100 cases after training based on a set of 466 cases. Figure 6 presents the normalized confusion matrix obtained for the Shenzhen dataset, we achieve an overall accuracy of **98.3%** in this scenario. An IOU value of **0.95** is obtained. Figure 7 presents the result obtained using the U-Net architecture. Figure 8 compares the pixel by pixel output obtained using our proposed U-Net algorithm with the ground truth (hand drawn) for an example case. Results obtained using U-Net architecture for both datasets are summarized in Table 6.

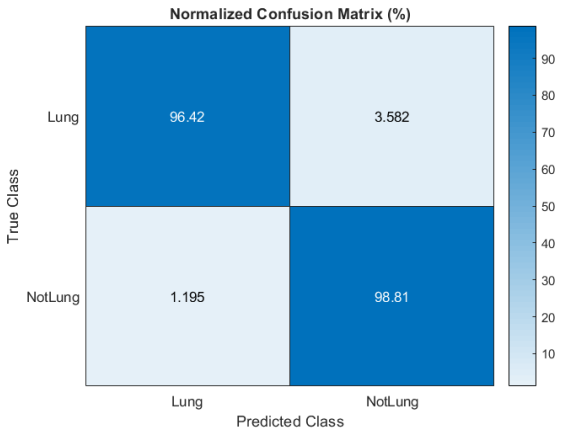

Figure 6: Normalized Confusion Matrix obtained for Shenzhen Dataset (100 test cases)

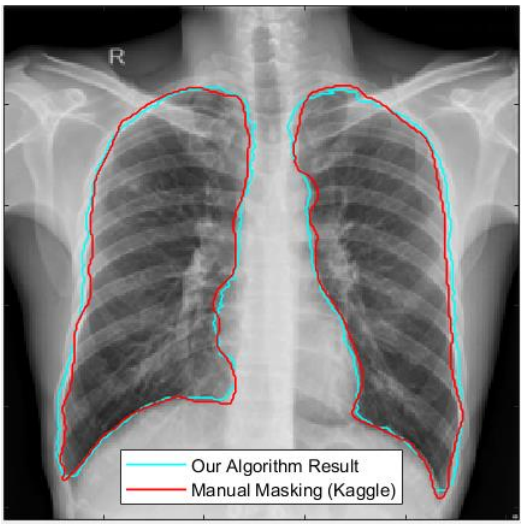

Figure 7: U-Net result obtained for an example case from the Shenzhen database

Table 6: Summary of Results for Test Datasets

Test Database	Pixel-based Classification accuracy (%)	IOU	Computation time (Entire test set) (Seconds)
JRST (140 cases)	95.7	0.92	11.5
Shenzhen (100 cases)	98.3	0.95	8

Figure 8: Difference between the manual lung mask and mask obtained using our proposed algorithm for an example case from the Shenzhen database.

Results obtained for 100 test cases present in the Shenzhen dataset is presented in [24]. Computation time for the **entire set of 100 test cases** on a laptop with i7 processor @ 2.8 GHz with 16 GB RAM and NVIDIA GeForce GTX 1070 is **8 seconds**. Table 7 presents the IOU scores of other algorithms proposed in the literature for JRST dataset. Table 7 indicates that anatomical atlases algorithm [13] outperforms other approaches. Table 8 compares the performance and computation time for lung segmentation using the proposed algorithm and anatomical atlases algorithm.

Table 7: IOU Scores of Algorithm reported in literature

Algorithm	**IOU Scores**
Anatomical Atlases [13]	**0.95**
Hybrid Voting [14]	0.94
ASM-tuned [14]	0.90
Fuzzy-curve [15]	0.92
Mean shape [14]	0.71
ASM – SIFT [16]	0.71

Table 8: Performance Comparison in terms of IOU and Computation Time for JRST dataset

Algorithm	IOU Scores	Computation time per case (Seconds)
Anatomical Atlases	0.95	20-25
Proposed Approach	0.92	**0.08**

V. CONCLUSIONS

In this paper, we have presented a novel computationally efficient and accurate lung segmentation algorithm for CRs. The algorithm provided good performance under different testing conditions proving its robustness and efficacy. A classification accuracy of 98.3% and IOU of 0.95 for Shenzhen dataset for a set of 100 CRs sets a new benchmark. Results obtained using U-Net for JRST database could serve as ground truth for future research efforts. Results indicate that performance on Shenzhen dataset is better than JRST dataset which could be due to the availability of large number of training cases in the Shenzhen dataset. Additionally, reduced performance on JRST database might be attributable to the algorithm being trained on imperfect ASM truth. Performance for JRST dataset can be improved further if we train our algorithm with a medical imaging expert marking the lung masks for both Riverain and JRST datasets.

Table 8 indicates that our proposed algorithm provides comparable performance (Difference in IOU is about 0.03) to the state-of-the-art algorithm for JRST dataset. However, our proposed algorithm is significantly faster (250x) than the anatomical atlases algorithm [13].

The lung segmentation algorithm presented in this paper could be utilized in computer aided detection systems for lung nodule detection and other similar applications. Obtaining highly accurate lung masks in a computationally efficient manner for a wide range of CRs would be of great benefit. Automated lung segmentation would be valuable for medical imaging experts and would enhance their workflow.

REFERENCES

[1] Duryea, J., & Boone, J. M. (1995). A fully automated algorithm for the segmentation of lung fields on digital chest radiographic images. *Medical Physics*, *22*(2), 183-191.

[2] Van Ginneken, Bram, Mikkel B. Stegmann, and Marco Loog. "Segmentation of anatomical structures in chest radiographs using supervised methods: a comparative study on a public database." *Medical image analysis* 10.1 (2006): 19-40.

[3] Armato III, Samuel G., Maryellen L. Giger, and Heber MacMahon. "Automated lung segmentation in digitized posteroanterior chest radiographs." *Academic radiology* 5.4 (1998): 245-255.

[4] Hardie, Russell C., et al. "Performance analysis of a new computer aided detection system for identifying lung nodules on chest radiographs." *Medical Image Analysis* 12.3 (2008): 240-258.

[5] Narayanan, Barath Narayanan, Russell C. Hardie, and Temesguen M. Kebede. "Analysis of various classification techniques for computer aided detection system of pulmonary nodules in CT." *Aerospace and Electronics Conference (NAECON) and Ohio Innovation Summit (OIS), 2016 IEEE National*. IEEE, 2016.

[6] Narayanan, Barath Narayanan, Russell C. Hardie, and Temesguen M. Kebede and Matthew J. Sprague. "Optimized feature selection-based clustering approach for computer-aided detection of lung nodules in different modalities." *Pattern Analysis and Applications*, 22(2), 559-571 (2019).

[7] Narayanan, Barath Narayanan, Russell C. Hardie, and Temesguen M. Kebede. "Performance Analysis of Feature Selection Techniques for Support Vector Machine and its Application for Lung Nodule Detection." *NAECON 2018-IEEE National Aerospace and Electronics Conference*. IEEE, 2018.

[8] Narayanan, Barath Narayanan, Russell Craig Hardie, and Temesguen Messay Kebede. "Performance analysis of a computer-aided detection system for lung nodules in CT at different slice thicknesses." *Journal of Medical Imaging* 5.1 (2018): 014504.

[9] Litjens, Geert, et al. "A survey on deep learning in medical image analysis." *Medical image analysis* 42 (2017): 60-88.

[10] Islam, Jyoti, and Yanqing Zhang. "A novel deep learning based multi-class classification method for Alzheimer's disease detection using brain MRI data." International Conference on Brain Informatics. Springer, Cham, 2017.

[11] Islam, Jyoti, and Yanqing Zhang. "Brain MRI analysis for Alzheimer's disease diagnosis using an ensemble system of deep convolutional neural networks." *Brain informatics* 5.2 (2018): 2.

[12] Ronneberger, Olaf, Philipp Fischer, and Thomas Brox. "U-net: Convolutional networks for biomedical image segmentation." *International Conference on Medical image computing and computer-assisted intervention*. Springer, Cham, 2015.

[13] Candemir, Sema, et al. "Lung segmentation in chest radiographs using anatomical atlases with nonrigid registration." *IEEE transactions on medical imaging* 33.2 (2014): 577-590.

[14] Van Ginneken, Bram, Mikkel B. Stegmann, and Marco Loog. "Segmentation of anatomical structures in chest

radiographs using supervised methods: a comparative study on a public database." *Medical image analysis* 10.1 (2006): 19-40.

[15] Coppini, Giuseppe, et al. "A computer-aided diagnosis approach for emphysema recognition in chest radiography." *Medical engineering & physics* 35.1 (2013): 63-73.

[16] Shi, Yonghong, et al. "Segmenting lung fields in serial chest radiographs using both population-based and patient-specific shape statistics." *IEEE Transactions on Medical Imaging* 27.4 (2008): 481-494.

[17] Shiraishi, Junji, et al. "Development of a digital image database for chest radiographs with and without a lung nodule: receiver operating characteristic analysis of radiologists' detection of pulmonary nodules." *American Journal of Roentgenology* 174.1 (2000): 71-74.

[18] Jaeger S, Karargyris A, Candemir S, Folio L, Siegelman J, Callaghan F, Xue Z, Palaniappan K, Singh RK, Antani S, Thoma G, Wang YX, Lu PX, McDonald CJ. "Automatic tuberculosis screening using chest radiographs". *IEEE Trans Med Imaging*. 2014 Feb;33 (2):233-45. doi: 10.1109/TMI.2013.2284099. PMID: 24108713

[19] Candemir S, Jaeger S, Palaniappan K, Musco JP, Singh RK, Xue Z, Karargyris A, Antani S, Thoma G, McDonald CJ. Lung segmentation in chest radiographs using anatomical atlases with nonrigid registration. *IEEE Trans Med Imaging*. 2014 Feb;33(2):577-90. doi: 10.1109/TMI.2013.2290491. PMID: 24239990

[20] Krizhevsky, Alex, Ilya Sutskever, and Geoffrey E. Hinton. "Imagenet classification with deep convolutional neural networks." *Advances in neural information processing systems*. 2012.

[21] He, K., X. Zhang, S. Ren, and J. Sun. "Delving Deep Into Rectifiers: Surpassing Human-Level Performance on ImageNet Classification." *Proceedings of the IEEE International Conference on Computer Vision*. 2015, 1026–1034.

[22] Noh, Hyeonwoo, Seunghoon Hong, and Bohyung Han. "Learning deconvolution network for semantic segmentation." *Proceedings of the IEEE international conference on computer vision*. 2015.

[23] U-Net Architecture Implementation in MATLAB, https://www.mathworks.com/help/vision/ref/unetlayers.html, Accessed March 27, 2019.

[24] Lung Segmentation Results on Shenzhen Dataset, https://www.youtube.com/watch?v=v1eWWrswu6M, Accessed March 27, 2019.